Pyrene-fused dibenzoazatetracenes: synthesis, crystal structures, photophysical properties and their morphologies

Qingsong Wang, #[a] Wei Gao, #[a] Yan Chen,[a] Xiaohui Wang,[a] Jin Zeng,[a] Yiwei Liu,[a] Huijuan Ran,[b] Zhen Hu,[a] Jie Bai,[a] Xing Feng,*[a] Carl Redshaw,[c] Qing Chen,*[d] Jian-Yong Hu,*[b]

Dedication ((optional))

[a] Q. Wang, W. Gao, Y. Chen, X. Wang, J. Zeng, Y. Liu, Z. Hu, Dr. J. Bai, Dr. X. Feng
Guangdong Provincial Key Laboratory of Functional Soft Condensed Matter, School of Material and Energy, Guangdong University of Technology, Guangzhou 510006, P. R. China
E-mail: hyxhn@sina.com (X. Feng.)
[b] H. Ran, Prof. Dr. J.-Y. Hu
Shaanxi Key Laboratory for Advanced Energy Devices, School of Materials Science and Engineering, Shaanxi Normal University, Xi'an 710119, P. R. China
E-mail: *hujianyong@snnu.edu.cn* (J.-Y. Hu)
[c] Prof. Dr. C. Redshaw
Department of Chemistry, University of Hull, Cottingham Road, Hull, Yorkshire HU6 7RX, UK.
[d] Dr. Q. Chen
Chinese Research Academy of Environmental Sciences, No.8, Dayangfang, Beiyuan, Beijing, P. R. China.
E-mail: chenging9821@163.com (Q. Chen)

Supporting information for this article is given via a link at the end of the document.((Please delete this text if not appropriate))

Abstract: Molecular packing and microstructure can play a crucial role in the photophysical and electronic properties of organic semiconductor materials. This article presents six pyrene-fused dibenzoazatetracenes **3** and the relationship between their molecular structures and the emission, and as well as the morphology has been investigated. All of the compounds display an aggregation-caused emission effect due to the extended π-conjugation associated with the close π-π stacking in their crystal structures. In terms of fluorescence, the compounds emitted sky-blue emission with a maximum peak (λ_{maxem}) in the range 469-474 nm with a quantum yield (Φ_f) of 0.37-0.50 in solution. In the solid state, the emission maximum red-shifts to ~528 nm and possesses a relatively low quantum yield (< 0.16). In addition, the electronic effects of the terminal group show only a limited effect on the emission behavior. On the other hand, *tert*-butyl groups have been introduced at the pyrene core, and contribute to enhance the solubility of the compound, and also improve the quality of the morphology.

Introduction

Pyrene is an important member of the polycyclic aromatic hydrocarbons (PAHs), and possesses high fluorescence with excellent quantum yield, as well as high charge-carrier mobility in the solid state.[1] Azaacenes are nitrogen-containing PAH members, which have been widely applied in organic electronics, sensors and anion radicals, due to their excellent electronic properties with large π-conjugation.[2,3] Pyrene-fused azaacene, containing pyrene and pyrazine units, belongs to the *N*-heteroacenes family, which are electron-poor species, and are preferred materials for high-performance n-type active materials in OFETs.[4]

A large number of pyrene-based azaacenes are known which are prepared *via* the facile functionalization of the pyrene core.[5,6] However, extending the π-conjugation via strong the π-π stacking of pyrene-based azaacenes leads to poor solubility and this not only influences the opto-electronic properties, but also quenches the fluorescence.[7] In order to construct more soluble large π-conjugation pyrene-fused azaacenes, side chains or substituents, such as *tert*-butyl, *n*-alkyl,[8] triisobutylsilyl,[9] triisopropylsilyl moieties,[10,11] have been introduced into the molecular skeleton to block/restrict the packing.

In this way, many novel azaacenes were prepared from a pyrene core, and systems with as many as 30 linearly-fused aromatic rings with a size of 7.7 nm in length have been reported by Aurelio Mateo-Alonso *et al*.[12] Moreover, large 3D pyrene-fused *N*-heteroacenes have been synthesized with a diameter of 10.88 nm.[13] Increasing the intrinsic solubility is not only to enrich the members of the PAHs family, but also to improve the electrical properties of such potential organic semiconductor. For example, the expanded π-conjugated **Py-Acene-4CN** is an n-type semiconductor with an electron mobility of 6.84×10^{-4} cm^2 V^{-1} s^{-1};[14] and when triisopropylsilane units are introduced into the pyrene azacene core to improve the solubility, the electron mobility of **Py-sAza-S** was improved to 0.016 cm^2 V^{-1} s^{-1}.[15]

Herein, in order to understand the relationship between the substituent group and the molecular pack to the photophysical properties and morphology, a set of K-conjugated (4-, 5-, 9- and 10-position) pyrene-fused dibenzoazatetracenes **3** are presented which have been characterized by $^1H/^{13}C$ NMR spectroscopy, single crystal X-ray diffraction and high-resolution mass spectrometry. The X-ray diffraction (XRD) and Atomic Force Microscope (AFM) were carried out to examine the relationship between the terminal substituents/molecular structures *versus* the photophysical, molecular packing, morphology on varying the donor/acceptor/bulky groups of the terminal group of the pyrene-fused dibenzoazatetracenes frameworks.

Results and Discussion

Synthesis and characterization

The synthetic route used for the pyrene-fused dibenzoazatetracene derivatives **3a**-**d** is illustrated in Scheme 1. The Knoevenagel condensation reaction between 4,5-diones (**1**) and 4,5-dibromobenzene-1,2-diamine afforded intermediate **2** in high yield (86%).[16] This was then employed for the preparation of the desired pyrene-based azacene derivatives **3a-d** by a

Pd-catalyzed Suzuki cross-coupling reaction. Furthermore, to improve the solubility of the pyrene-fused dibenzoazatetracenes, *tert*-butyl groups were introduced at the 2,7-positions of pyrene; the new homologues **3e** and **3f** were synthesized following the previously reported method[7] and the molecular structures are exhibited for comparison, All of the compounds were also fully characterized by $^{1}H/^{13}C$ NMR spectroscopy and by single crystal X-ray diffraction. The photophysical properties were also investigated by UV-vis and fluorescence spectra in THF solution and in the solid state. Thermogravimetric analysis (TGA) revealed that all compounds **3** possessed high thermal stability with decomposition temperatures of 407 °C for **3a**, 428 °C for **3b**, 337 °C for **3c**, 561 °C for **3d**, respectively.

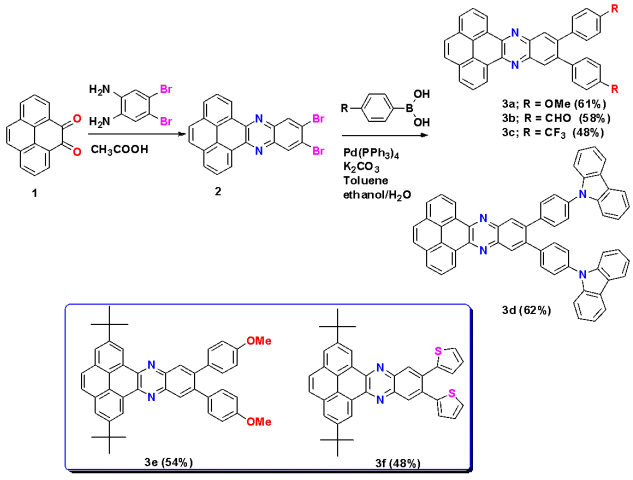

Scheme 1. Synthetic route to the pyrene-based azaacenes **3a-f.**

X-ray structure analysis

To gain detailed information on the molecular geometry of the new pyrene-fused dibenzoazatetracenes, crystals of **3a-c** suitable for X-ray diffraction analysis were cultivated from mixtures of hexane and CH_2Cl_2 at room temperature. Depending on the terminal group present, the crystal structures of **3a-c** adopted different molecular packing. The three molecules contain a flat pyrene core connecting twisted arylphenyl units. The details of the crystallographic parameters are listed in Table S3.

Crystal 3a: The compound **3a** crystallized in the monoclinic system with space group C 1 2/c 1. The expanded π-conjugation of the molecular skeleton involving all carbon and nitrogen atoms are in a plane with a twist angle of 0 °, while the terminal 4-methoxylphenyl group has a torsion angle of 51.4° toward the flat molecular fragment (Figure 1A). The twisted phenyl group is connected to a neighboring pyrene core forming a dimer structure *via* C-H···π interactions (C2-H14···C14 = 2.98 Å and C3-H17···C17 = 2.87 Å). Thus, the crystal **3a** adopts a face-to-face π-π stacking interaction with molecules above and below using phenyl carbons and a portion of the pyrene core interaction (Figure 1B), and the distance of π-π interactions between molecules is ~ 4.40 Å, which is weaker than that reported for other pyrene-based derivatives.[17] As shown in Figure 1C, the structure **3a** is arranged as parallel columns via head-to-tail π-π stacking along the *c*-axis.

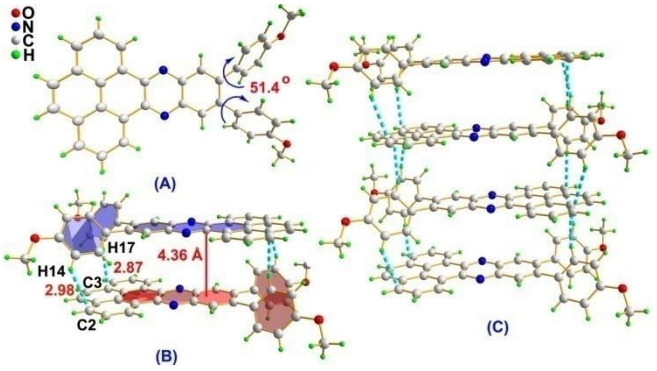

Figure 1 A) X-ray crystal structure of **3a**, B) the cofacial π-stacking at a distance of 4.36 Å and (C) the principal intermolecular packing interactions.

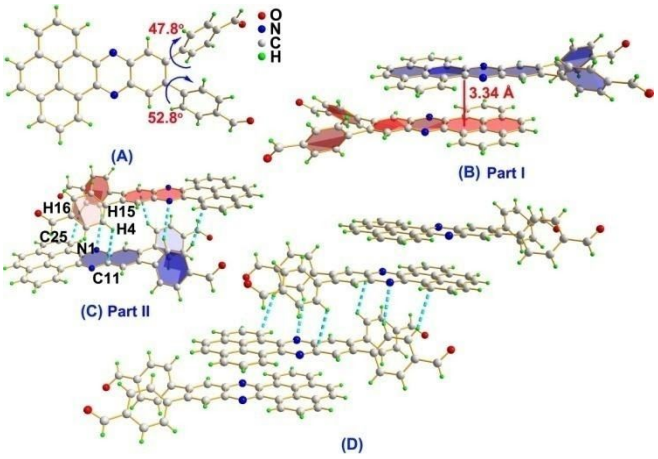

Figure 2 A) X-ray crystal structure of **3b**, B) and C) the details of the π-stacking in the structure and (D) the principal intermolecular packing interactions.

Crystal 3b: The crystal **3b** belongs to the triclinic system with the space group P-1, and the asymmetric unit contains one pyrene-azaacence molecule and one dichloromethane solvent molecule. Similarly, the molecule still retains a largely coplanar structure with a large π-conjugated molecular skeleton. The terminal 4-formylphenyl units are twisted around the C8-C15 bond and C9-C10 bonds in opposite directions, and the torsion angle is 47.8° for the C9-C10 bonds and 52.8° for the C8-C15 bond between the phenyl ring and molecular skeleton, respectively (Figure 2A). In the packing structure, as shown in Figure 2B and 2C, Part I adopts a close face-to-face π-π stacking between adjacent stacks using the whole extended π-conjugated molecular skeleton with a distance of ~3.32Å, while Part II adopts a face-to-edge herringbone arrangement with minimal π-overlap and are connected by numerous weak C-H···π bonds (C4-H4···C11 = 2.85 Å, C15-H15···N = 2.88 Å and C16-H16···C25 = 2.86 Å). More importantly, a 2D slipped packing pattern is formed by alternating Part Is and Part IIs along the *c*-axis in the crystalline structure.

Crystal 3c: The molecule **3c** crystallized in an orthorhombic crystal system with the centrosymmetric space group Pbcn, where the 4-position of the phenyl group is occupied by the trifluoromethyl (-CF_3) group. The crystal structure of **3c** revealed a different packing arrangement compared to **3a** and **3b**. Two polymorphs (Part I and Part II in Figure 3B and 3C) were observed in the crystal lattice. Part I features face-to-edge π-π stacking between two neighboring pyrene cores at a distance of 3.37 Å along the *a*-axis. Part II is also characterized by face-to-face π-π interactions above and below the molecular

azaacene core at a distance of ~3.72 Å. Thus, the two strong π-π interactions patterns were closely arranged to form a 2D column-like mode by alternating Part I and Part II polymorphs along the *b*-axis in the crystal structure (Figure 3D).

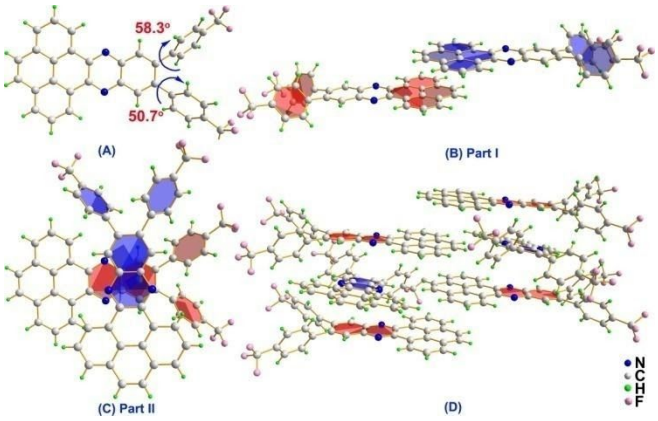

Figure 3 A) X-ray crystal structure representation of **3c**, B) and C) details of the π-stacking in the structure and (D) the principal intermolecular packing interactions.

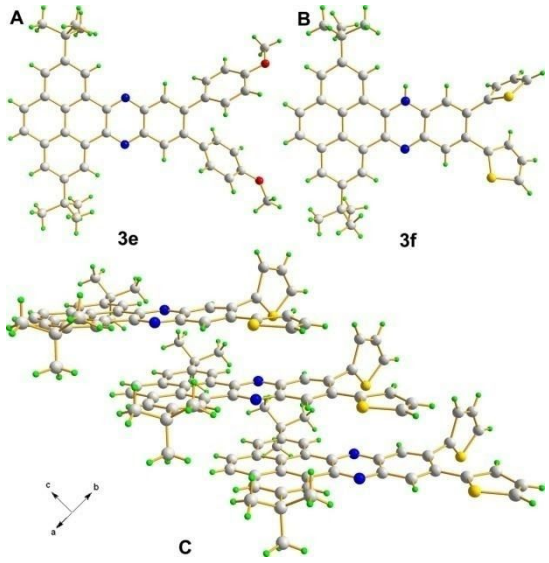

Figure 4 A) and B) X-ray crystal structure representations of **3e** and **3f**, B) and C) details of the π-stacking in the packing structure of **3f**.

Crystals 3e and 3f: Recrystalllization in a mixture of chloroform and hexane afforded high quality single crystals of the compound **3e**, whilst crystals of **3f** were prepared under several experiment conditions, but only CH_2Cl_2 solution afforded a small needle-like crystal suitable for diffraction but with a low quality crystalline structure. The X-ray single crystal diffraction analysis revealed that the crystal **3e** is arranged in head-to-tail stacking fashion with several C-H···π interactions. In the case of **3f**, despite the steric effects of the bulky *tert*-butyl group at the 2,7-positions of pyrene, the molecules still adopts a clear π-π stacking interaction between the pyrene units with the pyrazine section of an adjacent molecule, and the distance is *ca*. 3.45 Å (Figure 4C), and the molecule is almost perpendicular to the adjacent molecule linked by weak S···S and C-H···π interactions (Figure S31).

Photophysical properties

The absorption and fluorescence spectra of the pyrene-azaacene derivatives **3a-f** were measured in THF and are listed in Figure 5; selected spectroscopic data are summarized in Table 1. All compounds display similar absorption behavior, due to their similar molecular skeletons. The maximum short absorption peak in the range 294–315 nm is mainly associated with an intramolecular π–π* transition, while the long wavelength absorption peaks located at 451-454 nm are assigned to the n−π* transitions of the substituents and the extended π-conjugated molecular frameworks. The corresponding molar absorption coefficients of the short and long absorption range from 52000-76000 and 22800-32200 cm^{-1} M^{-1}, respectively.

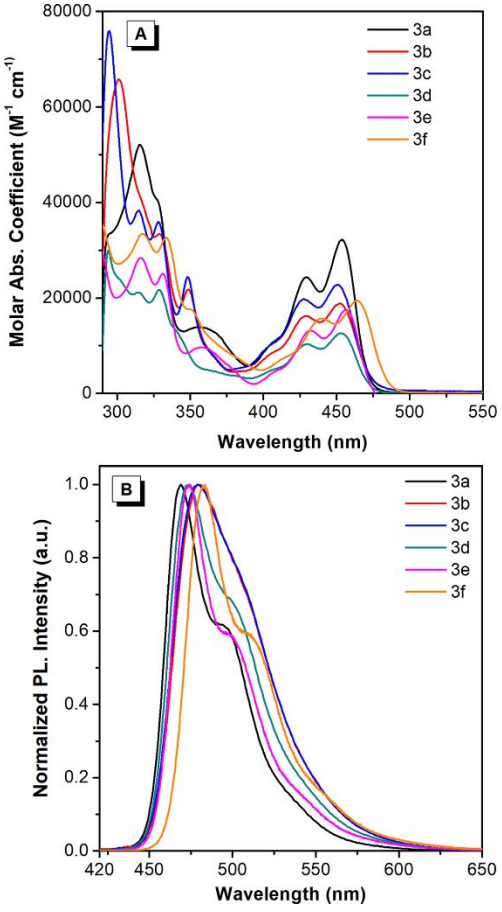

Figure 5 (A) UV-vis absorption and (B) normalized fluorescence spectra of compounds **3a-f** recorded in THF solutions at ~10^{-5} M at room temperature.

Table 1. The photophysical and electrochemical properties of **3**

Compd	λ_{maxabs} (nm) solns[a]	λ_{maxPL} (nm) solns[a]/ films[b]	Φ_F[c] solns[a]/ films[b]	HOMO (eV)[c]	LUMO (eV)[d]	ΔE (eV)	T_m[f]/T_d[g] (°C)
3a	454	469 / 511	0.46 / 0.08	-5.36 (-5.12)[d]	-2.10 (-2.49)	3.26[c] (2.63)e	268 / 406
3b	453	479 / 528	0.41 / 0.02	-5.80 (-5.09)	-2.59 (-2.47)	3.21 (2.62)	307 / 384
3c	451	474 / 488	0.37 / 0.16	-5.77 (-5.08)	-2.59 (-2.46)	3.18 (2.62)	310 / 333
3d	454	474 / 494	0.50 / 0.05	-5.33 (-5.29)	-2.37 (-2.65)	2.96 (2.63)	390 / 562
3e	453	476 / 521	0.52 / 0.14	-5.31 (nd)	-2.04 (nd)	3.27 (2.62)	nd / 416

3f	462	487 / 520	0.23 / 0.05	-5.44 (nd)	-2.23 (nd)	3.21 (2.56)	nd / 262

[a] Maximum absorption wavelength measured in THF at room temperature. [b] Measured in thin neat films. [c] Calculated by DFT/B3LYP/6-31G* using Gaussian 03 with values given in the brackets determined by CV using the ferrocene HOMO level. [d] Calculated from the empirical formula HOMO = - (4.8 + E_{ox}^{onset} - $E_{ox}^{onset}{}_{(Fc)}$), [e] calculated from the UV spectrum given in the brackets.. [f] Melting temperature (T_m) obtained from differential scanning calorimetry (DSC) measurements. [g] Decomposition temperature (T_d) obtained from thermogravimetric analysis (TGA). nd: not determination.

Tetraphenylpyrazine (TPP) and its derivatives,[18] show weak emission in solution but enhanced fluorescence intensity in the aggregate state, which defines them as aggregation-induced emission luminogens,[19]. Under excitation, the emission spectra of the pyrene-based compounds **3a**-**d** emit strong blue fluorescence with the maximum emission peak at 469-479 nm, and corresponding quantum yield values (Φ_f) of 0.37-0.46, respectively. The different electronic effects of the terminal groups (OMe, CHO, CF_3 and Carbazole) show only a slight effect on the absorption and fluorescence spectra in THF solvents for this extended π-conjugation pyrene-azaacene system. The concentration-dependent fluorescence of the pyrene-based azaacenes **3a**-**d** indicated that the emission peaks have red-shifted by about ~27 nm as the concentration increased from ~10^{-7} mol/L to ~10^{-3} mol/L (Figure S26). In comparison of the emission behavior, the fluorescence spectrum of **3e** exhibited a maximum emission peak at 476 nm in THF solution, which showed a slight red-shift (< 10 nm) compared to **3a**. Thus, the electron-donating group of the thienyl units in compound **3f** caused the maximum emission band shift to 486 nm. On the other hand, the thin film photoluminescence spectrum of the pyrene-azaacene derivatives exhibited a red-shifted emission band at 511nm for **3a**, 528 nm for **3b**, 488 nm for **3c** and 494nm for **3d**, respectively, along with a decreasing Φ_f value of 0.02-0.16, indicating that the extended π-conjugation molecular frameworks form stronger π-π intramolecular interactions and led to a red-shifted emission at high concentrations (>10^{-4} M) or in the solid state (Figure S26). Both compounds **3e** and **3f** exhibited a green fluorescence with a maximum emission band at *ca*. 520 nm in the solid state. (Figure S27) Thus, results indicated that the *tert*-butyl group at the 2,7-positions of pyrene exhibited a limited effect on the fluorescence behavior both in solution and in the solid state.

To more fully understand the self-assembly process, the temperature-dependent ^{1}HNMR spectra of the typical compound **3c** in d-DMSO solution were measured and are listed in Figure S28. As the temperature increased from 298 K to 358 K, the proton peaks at δ 9.43, 8.48, 8.21, 8.19 and 8.40 were shifted to low-field, and are assigned to the protons of the pyrene and the bridge of the phenyl ring, respectively. Therefore, we infer the planar molecules **3a-d** prefer to form aggregates via π-stacking,[20] which is consistent with their concentration-dependent fluorescence behavior and single crystal packing.

Furthermore, the effect of solvent polarity on the emission spectra of **3a**-**f** in different solvents, namely cyclohexane, dichloromethane, tetrahydrofuran, acetonitrile and dimethyl sulfoxide (DMSO) was explored. It was noticeable that the solvent polarity had a more pronounced effect on emission spectra rather than on the absorption spectra. As the solvent polarity increased from hexane to DMSO, the (Figure S29), the emission peak of compounds **3a** and **3d**–**3f** with donor-acceptor compounds exhibited a red-shift over the range 34-50 nm, due to the electron-rich nature of the aryl substituents. Importantly, the compound **3d** in DMSO displayed a dual emission peak at 495 and 593 nm, respectively. The longer emission wavelength maybe attributed to the intramolecular charge transfer (ICT) process in the strong polarity solvent.[21] In addition, in the presence of *t*-Bu units at the 2,7-positions, the fluorescence of **3e** and **3f** still exhibited a slight solvatochromic effect. The maximum emission bands were red-shifted *ca*. 39 nm in DMSO solution compared to in non-polarity solution (cyclohexane) (Table S2). According to their crystal packing structure, we infer that the J-aggregates plays a significant role to induce the red-shift of the emission peak.[22]

DFT calculations

To get insight into the molecular frontier orbitals and optimized molecular geometries of the pyrene-based azaacenes **3a**-**d**, theoretical calculations were performed by density functional theory (DFT) using the B3LYP functional and the 6-31G* basis set. As shown in Figure S34, although the presence of different electronic effects of terminal groups (such as OMe, CHO and CF_3), only shows a limited effect due to the electron density, both the HOMO and LUMO energy levels of **3a**-**c** are mainly located at the pyrene core and the pyrazine ring. The partial overlapped electronic density in the HOMO and LUMO levels led to weak intramolecular charge transfer (ICT) emission. However, the HOMO and LUMO levels in **3d** were clearly separated and were mainly at the pyrene-fused dibenzoazatetracenes ring and phenylcarbazole units, respectively. This led to an obvious ICT state in strong polarity solvents (e.g. DMSO). In addition, according to the DFT calculations, we found the presence of electron-withdrawn groups (CHO and CF_3) lowers the HOMO level and that the donor group is beneficial to enhancing the LUMO level, whilst the *tert*-butyl groups the 2,7-positions show a limited effect on the electron distribution; the detailed HOMO and LUMO levels are listed in Table 1. The energy band gap values of the pyrene-azaacene compounds **3a**-**f** are calculated to be in range from 2.96 eV to 3.27. Furthermore, the electrochemical behavior of the compounds 3 has been investigated by cyclic voltammetry with a scan rate of 0.1 V/s in dry CH_2Cl_2 using tetrabutylammonium hexafluorophosphate as electrolyte. The HOMO values were estimated from the first oxidation onset wave (E_{ox}^{onset}) by the empirical formula HOMO = - (4.8+E_{ox}^{onset} - $E_{ox}^{onset}{}_{(Fc)}$), the optical band gaps (E_g, 2.63 eV for **3a**, 2.61 eV for **3b**, 2.61 eV for **3c** and 2.63 for **3d**, respectively.) were derived from the onset wavelength of the absorption spectra in THF solution, and the corresponding LUMO levels were determined by the equation LUMO = HOMO + Eg. The HOMO and LUMO value of these compounds are summarized in Table 1 and the CV curves are presented in Figures S35-S38.

Morphology

To investigate the relationship between the molecular structure and the morphology, thin films of homogeneous **3a**-**f** on SiO_2/Si substrates were prepared according to previous reported.[23] The morphology of all the films was investigated by AFM. Figure 6 depicts the AFM images of the films **3a**-**f**, which exhibit a smooth, discontinuous surface with a clear boundary in the scanning area of 10 μm × 10 μm at room temperature, while the morphologies slightly change after annealing at 80 °C. The root-mean-squared (RMS) surface roughness value (Ra) of the corresponding films were 29.1, 10.2, 48.1, 4.66, 4.58 and 17.1 for **3a**-**f** at 25 °C, and 24.1, 20.3, 40.7, 8.04 1.29 and 10.1 nm for **3a**-**f** after annealing at 80 °C, respectively. Obviously, the compounds **3e** and **3f** exhibit good film forming ability on the SiO_2/Si substrates due to the enhanced solubility. The annealing process can improve the smoothness of the thin film. Furthermore, the morphology of thin film on the SiO_2/Si substrates was examined by X-ray diffraction (XRD) and atomic force microscopy (AFM) at 25°C and 80°C, respectively. The XRD characterization showed that the spin-coating films **3a-d** were of relative low crystallinity, and the XRD diffraction peak at 2θ = 21.7-23.2° is attributed to the strong π-π stacking in the range 3.86-4.40 Å, according to the equation (λ = 2d sinθ), respectively. These d-spacing values are in good agreement

with the π-π stacking which was observed from the crystal lattice. It is noteworthy that the sharp diffraction peak located at *ca.* 2θ = 33°, corresponds to d-spacings of *ca*. 2.71 Å, which maybe attributed to the intermolecular interactions, such as C-H ···π or hydrogen bonding.[24] Importantly, after annealing, the XRD characterization shows a similar diffraction peak as before, indicated that the morphologies of the films **3a**-**d** remain unchanged. Although the π-π stacking distance reduces from 3.86-4.40 Å in the films **3a**-**d** to 3.75-4.2 Å post-annealing according to XRD diffraction peak (2θ = 20.2-23.6°) (Figure S39), the π-π stacking interaction is still weaker than previously reported in pyrene chemistry.[25] In particular, the thin film still exhibits an amorphous-like pattern.

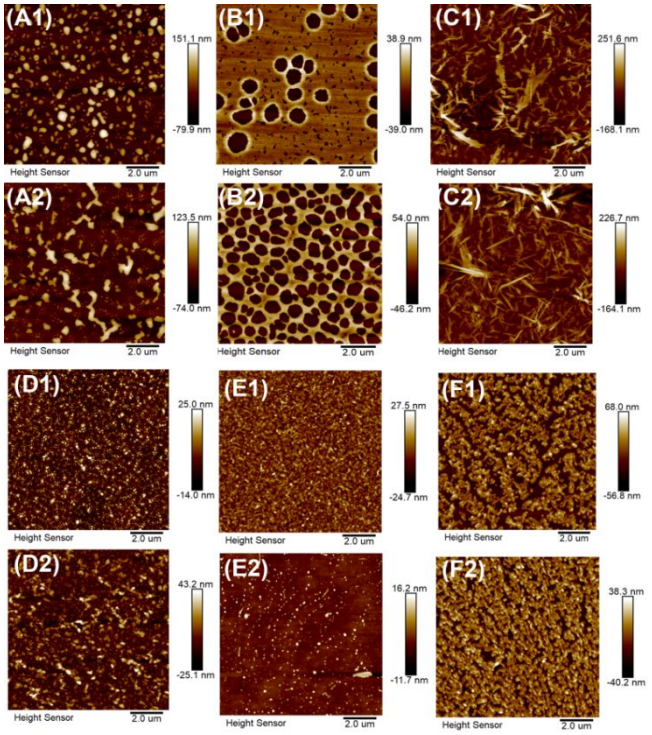

Figure 6 A1-F1) AFM image of pyrene-based azaacenes **3a-f** on a silica substrate at 25 °C, and **A2-F2)** AFM image of pyrene-based azaacenes **3a-f** on a silica substrate after annealing at 80 °C.

Conclusion

In this study, we have designed and synthesized six pyrene-fused dibenzoazatetracene compounds **3a-f** in order to investigate the relationship between the molecular structure, the molecular packing and the optical as well as the transistor properties. Firstly, all of the compounds exhibited blue emission (469-487 nm) in solution with relative high quantum yield, but due to the strong π-π stacking in the solid state, the pyrene-based compounds **3a-f** showed a clear ACQ effect with about 20-40 nm red shift and low quantum yield. Secondly, the substituent group in the terminal position of the large π-conjugated molecular skeleton exerts a limited effect on the emission behavior both in some polarity solvents and in the solid state; but the electronic effect would lead to an ICT process. Furthermore, on-going investigations are exploring an efficient approach to improve the high solubility of pyrene-based azaacence homologues and their morphologies; other larger π-conjugation molecular skeletons are also been explored for potential application in OFET devices.

Experimental Section

Materials: Unless otherwise stated, all other reagents used were purchased from commercial sources and were used without further purification.

Characterization: ^{1}H and ^{13}C NMR spectra were recorded on a Bruker AVANCE III 400M/600M spectrometer using chloroform-*d* solvent and tetramethylsilane as internal reference. *J*-values are given in Hz. High-resolution mass spectra (HRMS) were taken on a LC/MS/MS, which consisted of a HPLC system (Ultimate 3000 RSLC, Thermo Scientific, USA) and a TSQ Endura QQQ mass spectrometer. UV-vis absorption spectra and Photoluminescence (PL) spectra were recorded on a Shimadzu UV-2600 and the Perkin-Elmer LS 55 fluorescence spectrometer. PL quantum yields were measured using absolute methods using a Hamamatsu C11347-11 Quantaurus-QY Analyzer. Thermogravimetric analysis was carried on a Mettler Toledo TGA/DSC3+ under dry nitrogen at a heating rate of 10 °C/min. The quantum chemistry calculations were performed using the Gaussian 09W (B3LYP/6–31G* basis set) software package.[26]

X-ray Crystallography: Crystallographic data for the compounds was collected on a Bruker APEX 2 CCD diffractometer with graphite monochromated Mo Kα radiation (λ = 0.71073 Å) in the ω scan mode[27] The structures were solved by charge flipping or direct methods algorithms and refined by full-matrix least-squares methods on F^2.[28] All esds (except the esd in the dihedral angle between two l.s. planes) were estimated using the full covariance matrix. The cell esds were considered individually in the estimation of esds in distances, angles and torsion angles. Correlations between esds in cell parameters were only used when they were defined by crystal symmetry. An approximate (isotropic) treatment of cell esds was used for estimating esds involving l.s. planes. The final cell constants were determined through global refinement of the xyz centroids of the reflections harvested from the entire data set. Structure solution and refinements were carried out using the SHELXTL-PLUS software package.[28,29] Data (excluding structure factors) on the structures reported here have been deposited with the Cambridge Crystallographic Data Centre. CCDC 2005141-2005143, 2026734 and 2026735 contains the supplementary crystallographic data for this paper. These data could be obtained free of charge from The Cambridge Crystallographic Data Centre via www.ccdc.cam.ac.uk/data_request/cif.

Synthesis of pyrene-4,5-diones (1): A mixture of pyrene (1.0 g, 4.95 mmol) and sodium periodate (5.2 g, 24 mmol) in a mixture of THF (40 mL), dichloromethane (40 mL) and water (50 mL) was stirred at 0 °C under a nitrogen atmosphere for 10min., then ruthenium trichloride (0.15 g, 0.724 mmol) was added. After the mixture was continuously stirred over night at room temperature, it was poured into 200 mL water and filtered. The aqueous phase was extracted with dichloromethane twice (50 mL×2), the organic layer was combined and washed with water and brine, and dried with anhydrous Na_2SO_4 and evaporated. The residue was purified by column chromatography eluting with (CH_2Cl_2/hexane,1:1) to give pyrene-4,5-diones (**1**) (388 mg, 34%) as an orange-red powder. The NMR spectra is agreement with the previous reported. ^{1}H NMR (600 MHz, $CDCl_3$) δ 8.48 (dd, *J* = 7.4, 1.3 Hz, 2H), 8.17 (dd, *J* = 7.9, 1.3 Hz, 2H), 7.85 (s, 2H), 7.75 (t, *J* = 7.7 Hz, 2H).

Synthesis of 11,12-dibromophenanthro[4,5-abc]phenazine (2a): Compound **1** (120 mg, 0.52 mmol) and 4,5-dibromobenzene-1,2-diamine (159 mg, 0.60 mol) were dissolved in 10 mL of acetic acid and stirred under a nitrogen atmosphere, the mixture was stirred at 120 °C for 24 h. After it was cooled to room temperature, the reaction mixture was filtered and washed with ethanol (50 mL), and dried under vacuum. The residue (205 mg, 86%) was a yellow powder and was used without purification due to its low solubility.

Synthesis of 11,12-bis(4-methoxyphenyl)phenanthro[4,5-abc]phenazine (3a): Compound **2** (100 mg, 0.216 mmol), 4-methoxyphenyl boronic acid (83 mg, 0.54 mol), $Pd(PPh_3)_4$, (35 mg, 0.03 mmoL) and Na_2CO_3 (300 mg, 2.86 mmol) were mixed in a flask containing argon saturated toluene (10 mL), ethanol (2 mL) and H_2O (2 mL). Then the reaction mixture was refluxed for 24 h. After it was cooled to room temperature, the reaction mixture was extracted with dichloromethane (50 mL×2), and the organic layer was washed with H_2O and brine, and then dried with anhydrous Na_2SO_4 and evaporated. The residue was purified by column chromatography using dichloromethane as eluent to provide a yellow powder (68 mg, 61 %).^{1}H NMR (600 MHz, $CDCl_3$) δH: 9.61 (dd, J = 7.6, 1.0 Hz, 2H), 8.38 (s, 2H), 8.30 (dd, J = 7.7, 1.0 Hz, 2H), 8.11 (t, J = 7.7 Hz, 3H), 8.06 (s, 2H), 7.28 (d, J = 8.7 Hz, 4H), 6.88 (d, J = 8.7 Hz, 4H), 3.86 ppm (s, 6H); ^{13}C NMR (150 MHz, $CDCl_3$) δ 158.92, 143.44, 143.30, 141.76, 133.05, 131.46, 131.16, 130.07, 129.72, 129.12, 127.25, 126.89, 126.12, 123.91, 113.60, 55.27 ppm. MS (FAB) m/z: calcd for $C_{36}H_{24}N_2O_2$ 516.60; found 517.19189 [M^++1].

Synthesis of 4,4'-(phenanthro[4,5-abc] phenazine-11,12-diyl) dibenzaldehyde (3b): Compound **2** (100 mg, 0.216 mmol),

4-formylphenylboronic acid (150 mg, 0.646 mol), $Pd(PPh_3)_4$, (35 mg, 0.03 mmoL) and Na_2CO_3 (300 mg, 2.86 mmol) were mixed in a flask containing argon saturated toluene (10 mL), ethanol (2 mL) and H_2O (2 mL). Then the reaction mixture was refluxed for 24 h. After it was cooled to room temperature, the reaction mixture was extracted with dichloromethane (50 mL×2), and the organic layer was washed with H_2O and brine, and then dried with anhydrous Na_2SO_4 and evaporated. The residue was purified by column chromatography using V_{hexane}:V_{CH2Cl2}=1:2 as eluent to provide 4,4'-(phenanthro[4,5-abc] phenazine-11,12-diyl) dibenzaldehyde **(3b)** as a yellow powder (64 mg, 58 %)**.** ^{1}H NMR (600 MHz, $CDCl_3$) δH: 10.05 (s, 2H), 9.56 (d, J = 7.6 Hz, 2H), 8.45 (s, 2H), 8.30 (d, J = 7.6 Hz, 2H), 8.10 (t, J = 7.7 Hz, 2H), 8.04 (s, 2H), 7.85 (d, J = 8.0 Hz, 4H), 7.50 (d, J = 8.0 Hz, 4H) ppm; ^{13}C NMR (151 MHz, $CDCl_3$) δ 191.82, 146.26, 144.41, 141.73, 141.39, 135.25, 131.49, 131.16, 130.65, 129.70, 129.31, 127.30, 127.00, 126.25, 124.21 ppm.MS (FAB) m/z: calcd for $C_{36}H_{20}N_2O_2$ 512.57; found 513.16047 [M^++1].

Synthesis of 11,12-bis(4-(trifluoromethyl) phenyl)phenanthro[4,5-abc] phenazine (3c): Compound **2** (300 mg, 0.646 mmol), 4-(trifluoromethyl)phenylboronic acid (300 mg, 1.58 mmol), $Pd(PPh_3)_4$, (70 mg, 0.06 mmoL) and Na_2CO_3 (600 mg, 5.72 mmol) were mixed in a flask containing argon saturated toluene (15 mL), ethanol (4 mL) and H_2O (4 mL). Then the reaction mixture was refluxed for 24 h. After it was cooled to room temperature, the reaction mixture was extracted with dichloromethane (50 mL×2), and the organic layer was washed with H_2O and brine, and then dried with anhydrous Na_2SO_4 and evaporated. The residue was purified by column chromatography using dichloromethane as eluent to provide 11,12-bis(4-(trifluoromethyl)phenyl)phenanthro[4,5-abc] phenazine (**3c**) as a yellow powder (184 mg, 48 %). ^{1}H NMR (600 MHz, DMSO) δH: 9.52 (d, J = 7.6 Hz, 2H), 8.53 (d, *J* = 7.6 Hz, 2H), 8.50 (s, 2H), 8.26 (s, 2H), 8.23 (t, *J* = 7.7 Hz, 2H), 7.78 (d, *J* = 8.2 Hz, 4H), 7.62 (d, *J* = 8.0 Hz, 4H) ppm; ^{13}C NMR (150 MHz, $CDCl_3$) δ 144.37, 141.74, 141.32, 131.52, 131.21, 130.27, 129.67, 129.38, 127.31, 127.02, 126.28, 125.32, 124.21 ppm. MS (FAB) m/z: calcd for $C_{36}H_{18}F_6N_2$ 592.54; found 593.14570 [M^++1].

Synthesis of 11,12-bis(4-(9H-carbazol-9-yl)phenyl)phenanthro[4,5-abc] phenazine (3d): Compound **2** (100 mg, 0.216 mmol), 4-(9H-carbazol-9-yl) phenylboronic acid (185 mg, 0.646 mol), $Pd(PPh_3)_4$, (35 mg, 0.03 mmoL) and Na_2CO_3 (300 mg, 2.86 mmol) were mixed in a flask containing argon saturated toluene (10 mL), ethanol (2 mL) and H_2O (2 mL). Then the reaction mixture was refluxed for 24 h. After it was cooled to room temperature, the reaction mixture was extracted with dichloromethane (50 mL×2), and the organic layer was washed with H_2O and brine, and then dried with anhydrous Na_2SO_4 and evaporated. The residue was purified by column chromatography using dichloromethane as eluent to provide 11,12-bis(4-(9H-carbazol-9-yl)phenyl)phenanthro[4,5-abc]phenazine (**3d**) as a yellow powder (106 mg, 62 %). ^{1}H NMR (600 MHz, $CDCl_3$) δH 9.68 (dd, *J* = 7.6, 1.0 Hz, 2H), 8.65 (s, 2H), 8.35 (dd, *J* = 7.6, 1.0 Hz, 2H), 8.20 – 8.13 (m, 6H), 8.10 (s, 2H), 7.72 – 7.66 (m, 4H), 7.66 – 7.60 (m, 4H), 7.48 (d, *J* = 8.1 Hz, 4H), 7.42 – 7.37 (m, 4H), 7.31 (dd, *J* = 10.9, 3.9 Hz, 4H). ^{13}C NMR (151 MHz, $CDCl_3$) δ 144.07, 142.49, 141.92, 140.76, 139.51, 137.04, 131.60, 131.53, 130.66, 129.58, 129.49, 127.32, 127.01, 126.76, 126.26, 126.14, 124.13, 123.51, 120.39, 120.12, 109.67 ppm.MS (FAB) m/z: calcd for $C_{58}H_{34}N_4$ 786.94; found 787.28529 [M^++1].

2,7-di-*tert*-butyl-11,12-bis(4-methoxyphenyl)phenanthro[4,5-abc]phenazine (3e): 11,12-dibromo-2,7-di-*tert*-butylphenanthro[4,5-abc]phenazine (200 mg, 0.350 mmol), 4-methoxyphenylboronicacid (193 mg,1.40 mol), $Pd(PPh_3)_4$, (35 mg, 0.03 mmoL) and Na_2CO_3 (300 mg, 2.86 mmol) were mixed in a flask containing with argon saturated toluene (15 mL), ethanol (4 mL) and H_2O (4 mL). Then the reaction mixture was refluxed in 90 ℃ for 24 h. After it was cooled to room temperature, the reaction mixture was extracted with dichloromethane (50 mL), and the organic layer was washed with H_2O and brine, and then dried with anhydrous Na_2SO_4 and evaporated. The residue was purified by column chromatography using hexane:dichloromethane = 1:1 as eluent to provide a yellow powder 118 mg (54%). ^{1}H NMR (600 MHz, $CDCl_3$) δ 9.66 (d, *J* = 1.5 Hz, 2H), 8.41 (s, 2H), 8.27 (d, *J* = 1.5 Hz, 2H), 8.00 (s, 2H), 7.29 (d, *J* = 8.5 Hz, 4H), 6.87 (d, *J* = 8.5 Hz, 4H), 3.85 (s, 6H), 1.66 (s, 18H) ppm. ^{13}C NMR (150 MHz, $CDCl_3$) δ 158.83 (s), 149.67 (s), 143.91 (s), 142.88 (s), 141.50 (s), 133.20 (s), 131.18 (s), 130.16 (s), 129.13 (s), 127.26 (s), 125.71 (s), 124.21 (s), 121.39 (s), 113.54 (s), 77.23 (s), 77.01 (s), 76.80 (s), 55.26 (s), 35.53 (s), 31.88 (s) ppm. MS (FAB) m/z: calcd for $C_{44}H_{40}N_2O_2$ 628.82; found 629.31592 [M^++1].

Synthesis of 2,7-di-*tert*-butyl-11,12-di(thiophen-2-yl)phenanthro[4,5-abc] phenazine (3f): 11,12-dibromo-2,7-di-*tert*-butylphenanthro[4,5-abc]phenazine (200 mg, 0.350 mmol), 4-thienlyboronicacid (127 mg,1.74 mol), $Pd(PPh_3)_4$, (35 mg, 0.03 mmoL) and Na_2CO_3 (300 mg, 2.86 mmol) were mixed in a flask containing with argon saturated toluene (15 mL), ethanol (4 mL) and H_2O (4 mL). Then the reaction mixture was refluxed in 90 ℃ for 24 h. After it was cooled to room temperature, the reaction mixture was extracted with dichloromethane (50 mL), and the organic layer was washed with H_2O and brine, and then dried with anhydrous Na_2SO_4 and evaporated. The residue was purified by column chromatography using dichloromethane as eluent to provide a powder 97 mg (48%). ^{1}H NMR (400 MHz, $CDCl_3$) δ 9.63 (t, *J* = 2.0 Hz, 2H), 8.59 – 8.42 (m, 2H), 8.28 (d, *J* = 1.3 Hz, 2H), 8.06 – 7.92 (m, 2H), 7.41 (d, *J* = 5.0 Hz, 2H), 7.15 – 7.02 (m, 4H), 1.67 (d, *J* = 2.7 Hz, 18H). ^{13}C NMR (100 MHz, $CDCl_3$) δ 149.77, 144.50, 141.74, 141.36, 135.80, 131.18, 130.94, 128.89, 128.09, 127.29, 127.20, 126.81, 126.03, 124.29, 121.64, 35.55, 31.89 ppm. MS (FAB) m/z: calcd for $C_{38}H_{32}N_2S_2$ 580.8080; found 581.20782 [M^++1].

Acknowledgements

Q. W and W. G contributed equally to this work. This work was supported by the National Natural Science Foundation of China (21975054 and 21602014), Natural Science Foundation of Guangdong Province of China (2019A1515010925), Guangdong Province Training Program of Innovation and Entrepreneurship for Undergraduates, “One Hundred Talents Program”of the Guangdong University of Technology (GDUT) (1108-220413205), Guangdong provincial key laboratory of functional soft condensed matter of the Guangdong University of Technology (GDUT) (220413205). CR thanks the EPSRC for an Overseas Travel Grant (EP/R023816/1).

Keywords: pyrene • crystal structure • structure-properties • morphologies • organic electronic

[1] a) T. M. Figueira-Duarte, K. Müllen, *Chem. Rev*. **2011**, *111*, 7260-7314; b) M. M. Islam, Z. Hu, Q. S. Wang, C. Redshaw, X. Feng, *Mater. Chem. Front.* **2019,** *3*, 762-781.
[2] U. H. F. Bunz, J. Freudenberg, *Acc. Chem. Res.* **2019**, *52*, 1575-1587.
[3] a) J. H. Chen, K. Yang, X. Zhou, X. G. Guo, *Chem. Asian. J.* **2018**, *13*, 2587-2600; b) U. H. F. Bunz, *Acc. Chem. Res.* **2015**, *48*, 1676-1686.
[4] a) A. Mateo-Alonso, *Chem. Soc. Rev.* **2014**, *43*, 6311-6324; b) X. Feng, F. Iwanaga, J. Y. Hu, H. Tomiyasu, M. Nakano, C. Redshaw, M. R. J. Elsegood, T. Yamato, *Org. Lett.* **2013**, *15*, 3594–3597; c) C. Li, H. Wonneberger, *Adv. Mater.* **2012**, *24*, 613-636.
[5] X. Feng, J.-Y. Hu, C. Redshaw, T. Yamato, *Chem. Eur. J.* **2016**, *22*, 11898-11916.
[6] X. Feng, J. Y. Hu, F. Iwanaga, N. Seto, C. Redshaw, M. R. J. Elsegood, T. Yamato, *Org. Lett.* **2013**, *15*, 1318-1321.
[7] a) N. Kulisic, S. More, A. Mateo-Alonso, *Chem. Commun.* **2011**, *47*, 514–516; b) A. Mateo-Alonso, N. Kulisic, G. Valenti, M. Marcaccio, Paolucci, F.; M. Prato, *Chem. Asian. J.* **2010**, 5, 482-485.
[8] B. X. Gao, M. Wang, Y. X. Cheng, L. X. Wang, X. B Jing, F. S. Wang, *J. Am. Chem. Soc.* **2008**, *130*, 8297-8306.
[9] S. More, S. Choudhary, A. Higelin, I. Krossing, M. Melle-Franco, A. Mateo-Alonso, *Chem. Commun.* **2014**, *50*, 1976-1979.
[10] W. Wu, Y. Liu, D. Zhu, *Chem. Soc. Rev.* **2010**, *39*, 1489-1502.
[11] Z. Zhao, S. Ye, Y. Guo, Z. Chang, L. Lin, T. Jiang, J. W.Y. Lam, P. Lu, H. Qiu, Y. Liu, B. Z. Tang, *Org. Electron.* **2011**, *12*, 2236–2242.
[12] D. Cortizo-Lacalle, J. P. Mora-Fuentes, K. Strutyński, A. Saeki, M. Melle-Franco, A. Mateo-Alonso, *Angew. Chem. Int. Ed.* **2018**, *57*, 703-708
[13] B. L. Hu, C. An, M. Wagner, G. Ivanova, A. Ivanova, M. Baumgarten, *J. Am. Chem. Soc.* **2019**, *141*, 5130-5134.
[14] M. M. Abadia, G. Antonicelli, E. Zuccatti, A. Atxabal, M. M. Franco, L,E. Hueso, A. M. Alonso, *Org. Lett.* **2017**, *19*, 1718−1721.
[15] A. B. Marco, D. Cortizo-Lacalle, C. Gozalvez, M. Olano, A. Atxabal, X. Sun, M. Melle-Franco, L. E. Hueso, *Chem. Commun.* **2015**, *51*, 10754-10757.
[16] a) P. K. Sahoo, C. Giri, T. S. Haldar, Rakesh. Puttreddy, K. Rissanen, P. Mal, Eur. J. Org. Chem. **2016**, 1283-1291. b) J. Hu, D. Zhang, F. W. Harris, *J. Org. Chem.* **2005**, *70*, 707-708
[17] a) M. Ashizawa, K. Yamada, A. Fukaya, R. Kato, K. Hara, J. Takeya, *Chem. Mater.* **2008**, *20*, 4883-4890; b) Y. C. Wu, Z. Y. Yin, J. C. Xiao, F. X. Wei, K. J. Tan, C. Kloc, L. Huang, Q. Y. Yan, F. Z. Hu, H. Zhang, Q. C. Zhang, *ACS. Appl. Mater. Interfaces.* **2012**, *4*, 1883-1886.
[18] M. Chen, L.Z. Li, H. Nie, J. Q. Tong, L. L. Yan, B. Xu, J. Z. Sun, W.J. Tian, Z. J. Zhao, A.J. Qin, B. Z. Tang, *Chem. Sci.* **2015**, *6*, 1932-1937.
[19] J. Mei, N. L. C. Leung, R. T. L. Kwok, J. W. Y. Lam, B. Z. Tang, *Chem. Rev.* **2015**, *115*, 11718-11940.
[20] M. Wang, Y. Li, H. Tong, Y.X. Cheng, L. X. Wang, X. B. Jing, F. Wang, *Org. Lett.* **2011**, *13*, 4378–4381.
[21] J. Yang, M. Li, L. Kang, W. Zhu, *Sci. China. Chem.* **2017**, *60*, 607–613.
[22] B. K. An, J. Gierschner, S.Y. Park, *Acc. Chem. Res.***2012**,45,544-554.
[23] K. Zhang, P. Wucher, T. Marszalek, M. Babics, A. Ringk, P. W. M. Blom, P. M. Beaujuge, W. Pisula, *Chem. Mater.* **2018**, *30*, 5032−5040.
[24] G. F. Lu, Y. L. Chen, Y. X. Zhang, M. Bao, Y.Z. Bian, X. Y. Li, J. Z. Jiang, *J. Am. Chem. Soc,* **2008**, *130*, 11623-11630.
[25] X. Feng, J. Y. Hu, L. Yi, N. Seto, Z. Tao, C. Redshaw, M. R. J. Elsegood, T. Yamato, *Chem. Asian. J.***2012**, 2854-2863.

[26] M. J. Frisch, G. W. Trucks, H. B. Schlegel, G. E. Scuseria, M. A. Robb, J. R. Cheeseman, Gaussian 09: Revision A. 02; Gaussian: Inc: Wallingford, CT, **2009**
[27] SAINT and APEX 2. Software for CCD diffractometers. Madison, USA: Bruker AXS Inc.**2015**.
[28] a) G. M. Sheldrick, *Acta. Cryst.* **2008**, *A64*, 112–122; b) G. M. Sheldrick, *Acta. Cryst.* **2015**, *A71*, 3–8.
[29] S. P. Westrip, *J. Appl. Cryst.* **2010**, *43*, 920–925.

Entry for the Table of Contents

Insert graphic for Table of Contents here. ((Please ensure your graphic is in **one** of following formats))

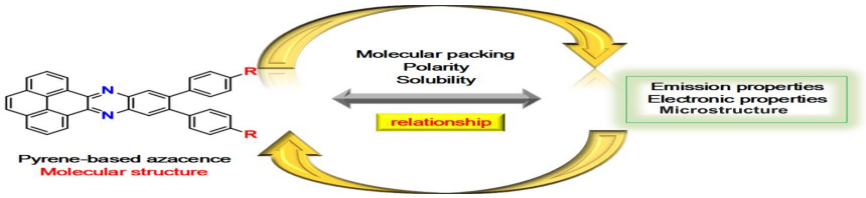

A set of pyrene-fused dibenzoazatetracenes **3** were synthesized and their relationship between their crystal structures and the emission, as well as morphology, has been detail investigated.

Figures and Tables

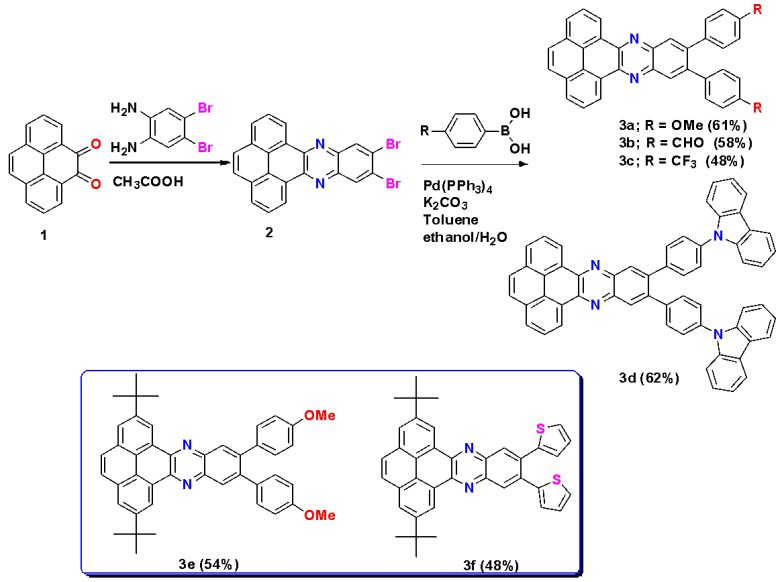

Scheme 1. Synthetic route to the pyrene-based azaacenes**3a-f.**

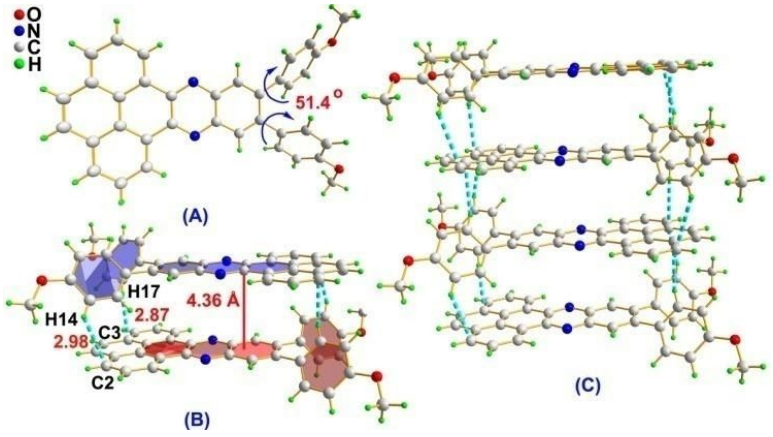

Figure 1 A) X-ray crystal structure of **3a**, B) the cofacial π-stacking at a distance of 4.36 Å and (C) the principal intermolecular packinginteractions.

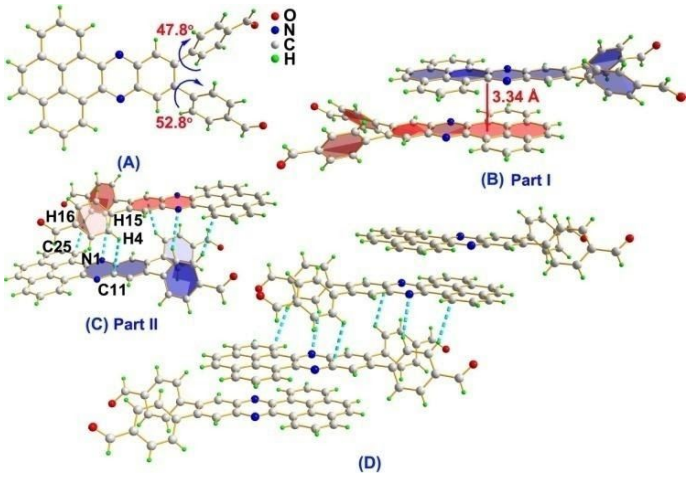

Figure 2 A) X-ray crystal structure of **3b**, B) and C) the details of the π-stacking in the structure and (D) the principal intermolecular packing interactions.

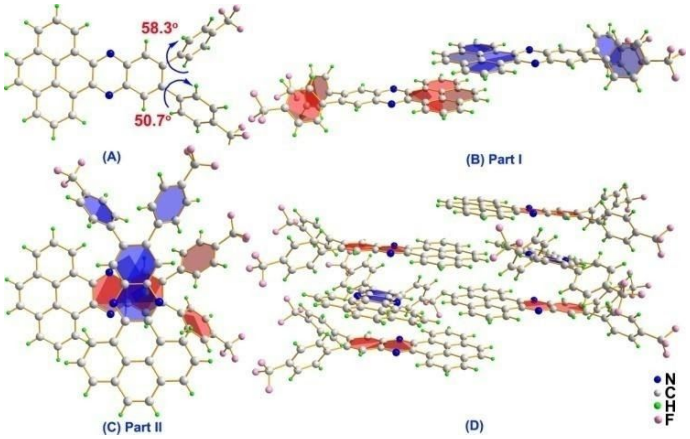

Figure 3 A) X-ray crystal structure representation of **3c**, B) and C) details of the π-stacking in the structure and (D) the principal intermolecular packing interactions.

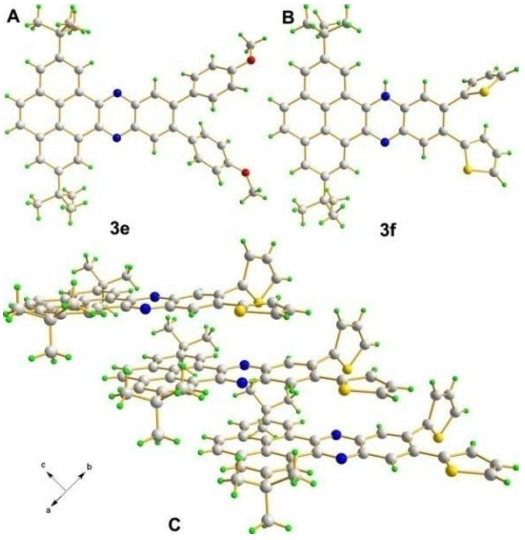

Figure 4 A) and B) X-ray crystal structure representations of **3e** and **3f**, B) and C) details of the π-stacking in the packing structure of **3f**.

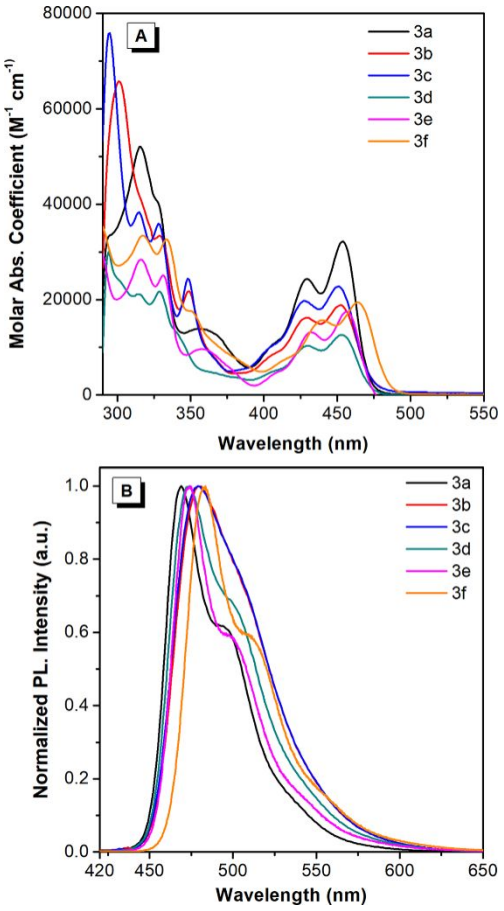

Figure 5 (A) UV-vis absorption and (B) normalized fluorescence spectra of compounds **3a-f** recorded in THF solutions at ~10^{-5} M at room temperature.

Table 1. The photophysical and electrochemical properties of **3**

Compd	λ_{maxabs} (nm) solns[a]	λ_{maxPL} (nm) solns[a]/ films[b]	Φ_f[c] solns[a]/ films[b]	HOMO (eV)[c]	LUMO (eV)[d]	ΔE (eV)	T_m[f]/T_d[g] (°C)
3a	454	469 / 511	0.46 / 0.08	-5.36 (-5.12)[d]	-2.10 (-2.49)	3.26[c] (2.63)e	268 / 406
3b	453	479 / 528	0.41 / 0.02	-5.80 (-5.09)	-2.59 (-2.47)	3.21 (2.62)	307 / 384
3c	451	474 / 488	0.37 / 0.16	-5.77 (-5.08)	-2.59 (-2.46)	3.18 (2.62)	310 / 333
3d	454	474 / 494	0.50 / 0.05	-5.33(-5.29)	-2.37 (-2.65)	2.96 (2.63)	390 / 562
3e	453	476 / 521	0.52 / 0.14	-5.31(nd)	-2.04(nd)	3.27 (2.62)	nd / 416
3f	462	487 / 520	0.23 / 0.05	-5.44(nd)	-2.23(nd)	3.21 (2.56)	nd / 262

[a]Maximumabsorption wavelength measured in THF at room temperature. [b]Measured in thin neat films. [c] Calculated by DFT/B3LYP/6-31G* using Gaussian 03 with values given in the brackets determined by CV using the ferrocene HOMO level. [d] Calculated from the empirical formula HOMO = - (4.8 + E_{ox}^{onset} - E $ox^{onset}_{(Fc)}$), [e] calculated from the UV spectrum given in the brackets.. [f] Melting temperature (T_m) obtained from differential scanning calorimetry (DSC) measurements. [g] Decomposition temperature (T_d) obtained from thermogravimetric analysis (TGA). nd: not determination.

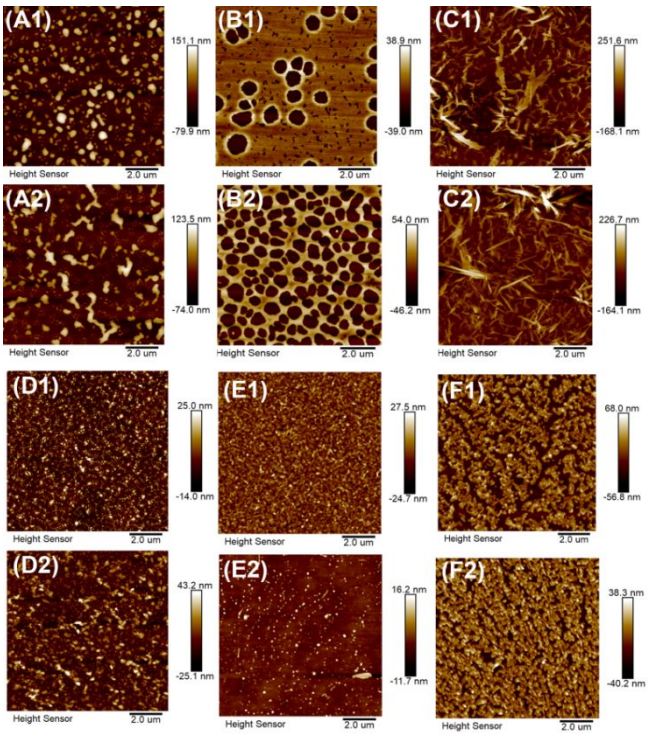

Figure 6 A1-F1) AFM image of pyrene-based azaacenes**3a-f** on a silica substrate at 25 ^{oC}, and **A2-F2)** AFM image of pyrene-based azaacenes**3a-f** on a silica substrate after annealing at 80 ^{o}C.